Structure, Vol. 11, 1537–1546, December, 2003, ©2003 Elsevier Science Ltd. All rights reserved. DOI 10.1016/j.str.2003.11.006

Insights into Cyclin Groove Recognition: Complex Crystal Structures and Inhibitor Design through Ligand Exchange

George Kontopidis,[1,*] Martin J.I. Andrews,[1] Campbell McInnes,[1] Angela Cowan,[1] Helen Powers,[1] Lorraine Innes,[1] Andy Plater,[1] Gary Griffiths,[1] Dougie Paterson,[2] Daniella I. Zheleva,[1] David P. Lane,[1] Stephen Green,[2] Malcolm D. Walkinshaw,[1,3] and Peter M. Fischer[1]

[1]Cyclacel Ltd.
James Lindsay Place
Dundee DD1 5JJ, Scotland
United Kingdom

[2]AstraZeneca Pharmaceuticals
Alderley Park
Macclesfield
Cheshire SK10 4TG
United Kingdom

[3]The University of Edinburgh
Michael Swann Building
King's Buildings
Edinburgh EH9 3JR, Scotland
United Kingdom

Summary

Inhibition of CDK2/CA (cyclin-dependent kinase 2/cyclin A complex) activity through blocking of the substrate recognition site in the cyclin A subunit has been demonstrated to be an effective method for inducing apoptosis in tumor cells. We have used the cyclin binding motif (CBM) present in the tumor suppressor proteins $p21_{WAF1}$ and $p27_{KIP1}$ as a template to optimize the minimal sequence necessary for CDK2/CA inhibition. A series of peptides were prepared, containing nonnatural amino acids, which possess nano- to micromolar CDK2-inhibitory activity. Here we present X-ray structures of the protein complex CDK2/CA, together with the cyclin groove-bound peptides H-Ala-Ala-Abu-Arg-Ser-Leu-Ile-(*p*-F-Phe)-NH_2 (peptide 1), H-Arg-Arg-Leu-Ile-Phe-NH_2 (peptide 2), Ac-Arg-Arg-Leu-Asn-(*m*-Cl-Phe)-NH_2 (peptide 3), H-Arg-Arg-Leu-Asn-(*p*-F-Phe)-NH_2 (peptide 4), and H-Cit-Cit-Leu-Ile-(p-*F*-Phe)-NH_2 (peptide 5). Some of the peptide complexes presented here were obtained through the novel technique of ligand exchange within protein crystals. This method may find general application for obtaining complex structures of proteins with surface-bound ligands.

Introduction

Human cancer cells are characterized by the loss of cell cycle checkpoint regulation, leading to cell proliferation under conditions where nontransformed cells cannot enter and pass through the cell cycle. CDKs and their natural inhibitors, the CDK tumor suppressor proteins (CDKIs), are central to cell cycle regulation and their functions are commonly altered in tumor cells (Ortega et al., 2002). Deregulation of CDK2 and CDK4 through inactivation of CDKIs such as $p16^{INK4a}$, $p21^{WAF1}$, $p27^{KIP1}$, and $p57^{KIP2}$ thus provides a means for cancer cells to override the G1 checkpoint. Reinstatement of CDK inhibition therefore represents an opportunity for pharmacological interference with tumor progression. This is particularly attractive as one consequence of unchecked CDK2 activity is persistent E2F transcriptional activity, which, unless terminated in a timely fashion during S-phase, constitutes a powerful apoptotic signal (Lees and Weinberg, 1999). Because E2F deactivation occurs through phosphorylation by CDK2/CA, tumor cells will be selectively sensitive to inhibition. One method of CDK2/CA inhibition is through the use of peptides that block binding of both pRb and E2F to the CDK2/CA complex (Fischer and Lane, 2000).

Recognition of both of these substrates, as well as CDKIs, by the CDK2/CA complex depends on a shallow hydrophobic surface binding site in the cyclin A subunit, termed the cyclin groove (Schulman et al., 1998). Recognition of this groove is mediated through certain sequences, designated the CBM (Chen et al., 1996). This motif represents a consensus of the cyclin groove binding sequences found in a variety of CDK2/CA partner proteins, including the CDKIs, pRb proteins, E2F transcription factors, p53, HDM2, the CDK-activating kinase CDK7, etc. This sequence is commonly referred to as the RXL or ZRXL motif, where Z and X denote basic residues (Fischer et al., 2003). Following a detailed study with peptides representing various sequences from cyclin A binding proteins, we recently refined the definition of the motif (McInnes et al., 2003): ZRXLYY′, where Y and Y′ are hydrophobic residues. The cyclin binding motif from p21 has also been examined by another group, which concluded that the motif is more accurately described as a cluster of hydrophobic residues covering the LYY′ portion of the sequence above (Wohlschlegel et al., 2001). However, other positions in the motif are seen and differences are observed in the relative importance of particular residues, most probably due to differences in experimental design.

When CBM peptides are conjugated to cellular delivery vectors (Fischer et al., 2001), the resulting peptide constructs cause cell cycle arrest and selective apoptosis in tumor cells in vitro (Ball et al., 1996; Bonfanti et al., 1997; Chen et al., 1999) and, as shown more recently, in vivo (Mendoza et al., 2003). Inhibition of CDK2 activity through blocking of substrate recruitment is also likely to provide kinase selectivity, which is more difficult to achieve with traditional ATP-competitive molecules (Fischer, 2001), since the cyclin-dependent substrate recognition, and hence phosphorylation, appears to be unique to CDKs 2 and 4.

A number of CDK2/CA complex X-ray crystal structures with CBM peptides have been reported. The first of these included a 68-residue $p27^{KIP1}$ fragment containing the ^{30}RNLFG^{34} sequence (Russo et al., 1996). A later study used a peptide with the sequence

*Correspondence: gkontopidis@cyclacel.com

^{658}RRLFGEDPPKE^{668} from p107, a pRb family protein (Brown et al., 1999). The most recent complexes reported included the peptides ^{376}STSRHKKLMFK^{386} (p53), ^{868}PPKPLKKLRFD^{878} (pRb), ^{25}KPSACRNLFGP^{35} (p27^{KIP1}), ^{87}PVKRRLDLE^{95} (E2F), and ^{653}AGSAKRRLFGE^{663} (p107) (Lowe et al., 2002). Our present work represents the first report using various peptides with the p21^{WAF1} motif ^{155}RRLIF^{159}.

In our recent work, comparison of a series of octapeptides derived from the p21^{WAF1} CBM-containing sequences, as well as those found in p107, E2F1, and p27^{KIP1}, showed (Zheleva et al., 2002) that the p21^{WAF1} ^{155}RRLIF^{159} motif was the most effective in cyclin A inhibitor peptides. In this motif the Arg^{155} residue was demonstrated to contribute extensively to binding. The optimized bioactive peptide H-His-Ala-Lys-Arg-Arg-Leu-Ile-Phe-NH_2, a low nanomolar CDK2/CA inhibitor (Zheleva et al., 2002), corresponds to the p21^{WAF1}(152-159) sequence, with a Ser^{153}-Ala mutation, which was found to enhance potency significantly. These observations rendered this sequence a good candidate for structural studies, as it provides the best template for the design of peptidomimetics. Herein we describe our initial approach toward the development of potent, smaller, and less peptidic inhibitors of CDK2/CA. We used the X-ray structures of these p21^{WAF}-derived peptide analogs, several of which were obtained through "ligand exchange," in conjunction with in vitro activity results to provide a comprehensive description of the requirements of each position in the CBM and to define a series of design principles for the structure-guided design of small molecule cyclin groove inhibitors.

Results and Discussion

In our previous work, we delineated the components of the p21^{WAF1} CBM (Zheleva et al., 2002) and arrived at a complete description of the motif through both extensive residue replacements, as well as by molecular modeling (McInnes et al., 2003). We proposed that residues C-terminal to the ZRXL motif are also critical for cyclin A binding and hence the motif would be better described by the sequence ZRXLYY′, where either Y and/or Y′ are hydrophobic residues. In this study, we were able to confirm this crystallographically and in addition, found that the ZRXLYY′ motif can be further truncated to RXLYY′, since the pentapeptide H-Arg-Arg-Leu-Ile-Phe-NH_2 retains considerable potency. In the present study, several CBM peptides, including those identified previously (McInnes et al., 2003), containing unnatural amino acids, which resulted in potency enhancements, were crystallized with CDK2/CA and their interactions with the cyclin groove described. The structural interpretation of the potency differences between various CBM peptides illustrates the determinants of cyclin groove binding and shows that small substitutions in the peptide structures can result in profound differences in activity and in the bound conformation.

In most cases it was not possible to cocrystallize complexes of the peptides with cyclin A and CDK2. To overcome this problem, we developed the novel technique of ligand exchange, in which a cocrystallized peptide is replaced by elution, followed by "soaking-in" a different inhibitor peptide. This approach, which may be of general utility in a variety of structural areas, is also described.

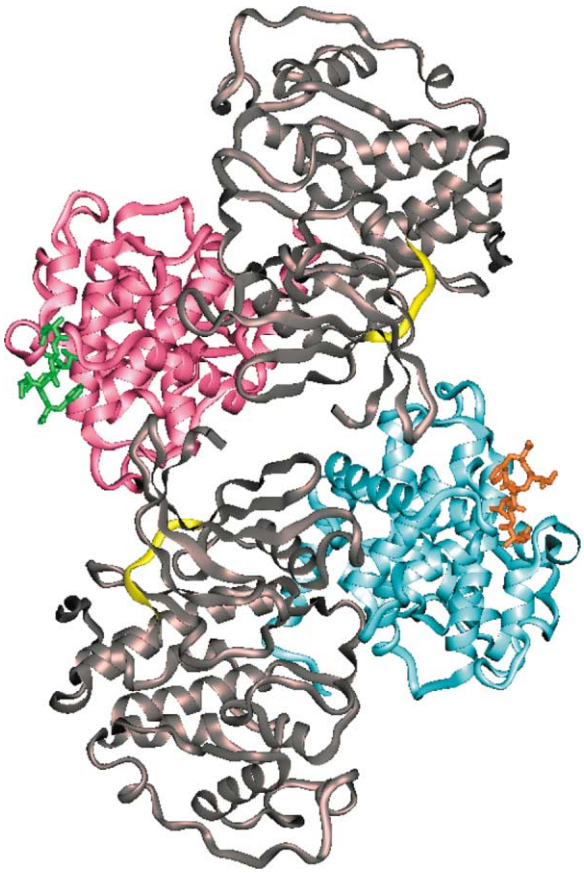

Figure 1. Ribbon Representation of the Noncrystallographic Dimer of the Ternary CDK2/CA/peptide 2 Complex

CDK2 molecules are shown in black, cyclin A subunits in pink and cyan. Bound peptides are colored green and orange. ATP binding sites are shown with yellow backbone atoms.

The peptide residue numbering system used throughout this work is based on the minimally active pentapeptide sequence, where amino acid residues are denoted Arg^1-Arg^2-Leu^3-Ile^4-Phe^5 and residues extending from the N and C termini are numbered −1 and 6, respectively. The cyclin groove components involved in binding specific residues are denoted similarly, e.g., site 1 for elements interacting with the residue at position (P^1) of the peptide ligand.

Crystal Soaking and Ligand Exchange

Initially, published crystallization conditions (Jeffrey et al., 1995) were employed. However, attempts to introduce peptides by soaking of these crystals were not successful and resulted in crystal lattice disorder and X-ray diffraction at a resolution of 5 Å at best. All peptide complex structures presented here were solved using a novel crystal form, which has space group $P2_12_12_1$ and contains two copies of the binary protein complex in the crystallographic asymmetric unit. Of the two peptide ligands in this complex, one (red in Figure 1) is fully

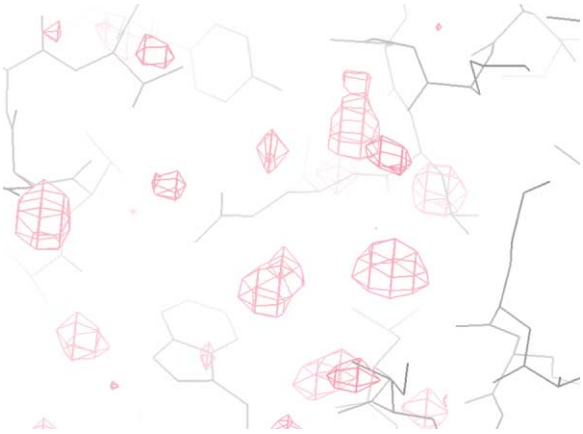

Figure 2. Replacement of One Peptide with Another in the CBG of a CDK2/CA Crystal

$1F_o - 1F_c$ difference electron density maps after 2 days soaking in mother liquor.

exposed to solvent channels in the crystal, while the second peptide site is partially occluded.

Peptides 2 and 4 were cocrystallized with CDK2/CA, while the remaining peptide complexes were prepared using the following ligand exchange procedure. A crystal containing H-Arg-Arg-Leu-Ile-Phe-NH_2 was soaked extensively against precipitant solution to elute the original peptide. Examination of electron density difference maps around the cyclin binding groove regions showed that the original cocrystallized peptide (Figure 3, peptide 2) had indeed been washed out (Figure 2). A second crystal was treated in the same way and then soaked in approximately 10 μl mother liquor solution containing 1 mM of a different peptide. The structure obtained showed that this peptide had been able to diffuse into the crystal lattice and to dock in the cyclin groove (Figure 3, peptides 1, 3, and 5). As the binding groove of one cyclin A molecule in the crystallographic unit is partially blocked by a neighboring CDK molecule, diffusion of the peptide ligand to this site was incomplete, even after 3 days of soaking. For this reason, ligand occupancy levels at the partially occluded binding groove are lower than at the free site in some of our structures. Due to this differential occupancy of the two sites in the asymmetric unit, only the fully accessible cyclin groove was used to compare the different bound peptide ligands. Crystallographic data for several novel $p21^{WAF1}$-derived peptide structures are summarized in Table 1.

Crystal-Ligand Exchange as a General Technique

The idea of soaking out ligands and leaving the crystal lattice intact, ready for reintroducing a new ligand, has been applied to metals and ions but the technique of "ligand exchange" has only rarely been applied to larger organic molecules (Munshi et al., 1998). Despite considerable efforts, we were not able to obtain crystals of uncomplexed CDK2/CA in the required crystal form and a ligand exchange protocol was developed that allowed us to examine a series of peptide complexes.

The most common application of crystal-soaking experiments is in the study of enzyme active site inhibitors. If crystals of the apo-enzyme are available, the technique of ligand exchange does not provide an obvious advantage over crystal soaking or cocrystallization with a given inhibitor. For nonenzymatic targets, it is more likely that protein recognition sites will be occupied by neighboring molecules in the crystal lattice. As we show here, cocrystallization of protein with a ligand, followed by "ligand exchange," may provide a more general way of studying binding sites involved in protein-protein interactions.

In general, the time required for ligand-soaking experiments can vary between seconds and days. In systems where no protein rearrangement is necessary (e.g., dipeptide ligands soaked into crystals of cyclophilin),

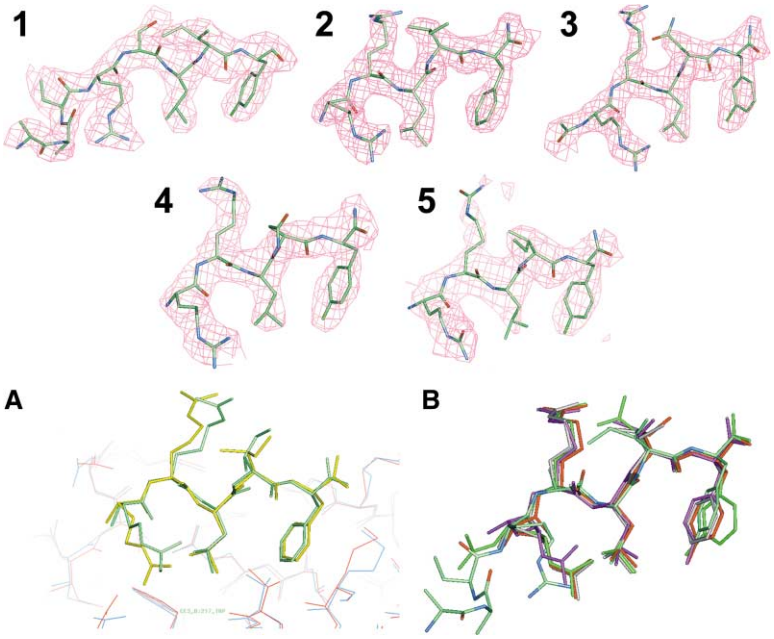

Figure 3. The Electron Density Maps of Peptides 1–5

The $2F_o - 1F_c$ maps are contoured at a level corresponding to 1.2 σ for the peptides bound to the nonoccluded cyclin groove.

(A) Superimposition of the structures of peptide 2 in the free (yellow) and partially occluded (green) CBG shows the differences of the two copies of the peptide.

(B) Overlay of the bound conformations of peptides 1 (gray), 2 (green), 3 (red), 4 (CPK coloring), and 5 (magenta).

Table 1. Crystallographic Data and Statistics

	Peptide				
	1	2	3	4	5
Data Collection					
Space group	$P2_12_12_1$	$P2_12_12_1$	$P2_12_12_1$	$P2_12_12_1$	$P2_12_12_1$
Unit cell (Å)					
a	74.5	74.2	74.5	73.5	74.5
b	114.6	113.9	114.0	113.0	113.5
c	157.0	155.3	156.2	153.1	154.5
Max. resolution (Å)	2.9	2.4	2.5	2.6	2.9
Observations	430,926	563,579	553,149	574,133	648,091
Unique reflections	31,043	52,345	46,855	39,765	29,357
Completeness (%)	84.6	96.7	99.0	99.5	98.9
R_{merge}[1]	0.10	0.11	0.10	0.11	0.12
Mean I/σ	8.7	5.9	4.9	5.8	2.8
Highest resolution bin	2.97-2.9	2.46-2.4	2.64-2.5	2.74-2.6	3.06-2.9
Mean I/σ (highest resolution bin)	1.4	1.2	1.0	1.0	1.5
R_{merge}[1] (highest resolution bin)	0.59	0.65	0.47	0.62	0.46
Refinement					
Protein atoms	8,924	8,924	8,924	8,924	8,924
Inhibitor atoms	124	100	108	102	102
Water	196	746	539	383	75
Reflections used in refinement	24,032	47,769	44,775	36,002	27,895
R_{factor}	19.3	19.7	17.2	19.6	20.2
R_{free}	29.2	27.8	25.3	28.9	29.1
Mean B-factor, protein ($Å^2$)	37.2	36.2	48.1	37.3	50.7
Mean B-factor, ligands ($Å^2$)	47.5	44.2	54.3	48.5	66.3
Mean B-factor, solvent ($Å^2$)	29.3	36.7	49.3	40.4	50.7

binding was found to take place within seconds (Wu et al., 2001). This contrasts with soaking times of days required for the binding of some CDK2 active site inhibitors, which require significant changes in the protein conformation before binding can occur (Wu et al., 2003). Diffusion of peptides in and out of the CDK2/CA crystals was slow and in some cases, even after a period of 3 days of soaking in new peptide solution, the original peptide could still be observed to occupy the binding groove. However, occasional agitation of the crystallization mixture during the 3-day period led to complete ligand exchange. Solution studies for peptides binding to the CBG using a competitive binding assay (McInnes et al., 2003) demonstrated that equilibrium is reached within a few seconds. Buffer and salt conditions in these solution studies and in the crystal exchange experiments described here were very similar, apart from the high PEG concentrations in the crystal soaking experiments. It therefore seems that diffusion rates play a major role during ligand exchange in crystals. It was fortuitous that the crystal system described has two ligand binding sites with different crystallographic environments, allowing us to obtain unambiguous results for the accessible site. Our results with this cyclin-CDK2 system suggest that the ligand exchange approach may be of general use in different protein systems where native protein crystals are not readily obtainable.

Overall Interactions between Ligand Peptides and Cyclin A

The binding site for the CBM peptides is comprised of a shallow groove resulting from the exposed surface of the cyclin A α1, α3, and α4 helices. The residues lining the groove form a number of subsites including the LYY′ hydrophobic pocket (Met^{210}, Ile^{213}, Leu^{214}, Trp^{217}, Leu^{253}), the arginine site (RX; Glu^{220}), and a secondary lipophilic pocket we call the alanine pocket (Val^{221}, Ile^{281}). In addition, binding is also facilitated by a number of H bond interactions with the peptide backbone, including a pair of interactions with the side chain carboxamide of Gln^{254}. Despite the well-documented observation that the CDK2 kinase subunit of the CDK2/CA complex undergoes significant conformational changes upon cyclin binding and T loop phosphorylation, the cyclin subunit structure is essentially the same in the free and complexed forms (Brown et al., 1995). In our peptide complex structures, most of the cyclin A binding groove (CBG) atoms are rigid and their average B factors do not change upon ligand binding. This was confirmed by comparison of the temperature factors of the CBG atoms with the rest of the cyclin A chain, as well as by comparison of the unliganded and peptide-liganded CDK2/CA structures. All main chain atoms of the residues in the groove have low B factors in both the peptide-bound and unliganded structures, although there are some significant differences in the side chains of the hydrophilic residues of the binding groove.

All residues in all of the peptide ligands complexes presented here are well defined by electron density. The electron density difference maps of the peptide complexes are shown in Figure 3. As mentioned, two CDK2/CA complexes exist in the asymmetric unit of our crystal form. The differences between the two copies of peptide 2 structures bound in the different CBGs are illustrated in Figure 3A. The RMS deviation for all atoms (50) after superimposition was 0.163 Å. Arg^{1}, Leu^{3}, and

Phe[5] make similar contacts in both cases, with some variation for Arg[2]. These variations should be considered in the context of the flexible Glu[220] receptor side chain and are discussed in more detail below. Ile[4] does not make contact with the binding groove and is restrained only through intramolecular contacts with Arg[2]. Arg[2] itself participates in charge-charge interactions with cyclin A, as well as some weak contacts with the neighboring CDK2 molecules in the case of the partially occluded CBG.

An overlay of all the solved peptide structures is shown in Figure 3B. Although the peptides bind in superficially similar modes, significant differences in inhibitory potency, and hence binding affinity, were observed between the peptides. These differences can be explained after detailed examination of the specific interactions formed or lost in each case, and are summarized below.

Peptide Potency and Design

Analysis of peptide 2 complexed with cyclin A shows that the bound conformation is stabilized through a number of contacts with the CBG, involving the side chains of Arg[1], Leu[3], and Phe[5], as well as the peptide backbone (Figure 4A). The latter include the Arg[1] terminal NH_2, Arg[1] CO, and Leu[3] NH groups. Judging from the interatomic distances, however, none of these form strong H bonds. Additionally, a number of intramolecular interactions involving Arg[1], Leu[3], and Phe[5] are observed. It is clear from the peptide crystal structures that residues P^1, P^3, and P^5 will be the main potency determinants, while P^2 and P^4, whose side chains project away from the binding groove, will be less important. Furthermore, the P^1, P^3, and P^5 side chains appear to form an intramolecular network of interactions. Thus, the side chains of Arg[1] and Phe[5] interact with the cyclin groove in such a way as to trap between them the Leu[3] side chain (Figure 4B1). The relative contribution to binding of each residue in the peptides can be judged from the activity summary in Table 2. It should be kept in mind when analyzing the potency data that the effect of any one mutation will be more profound in the context of a shorter than of a longer peptide.

P^1 Site

A key interaction in the CBM, and a requirement for good inhibitory potency of relevant peptides, is the ion pair between Glu[220] and Arg[1]. The importance of Arg in this position was also borne out in previous structures (Lowe et al., 2002), and mutation of Arg[1] always results in a decrease in biochemical inhibitory activity (McInnes et al., 2003). Even the isosteric substitution of Arg[1] with Cit[1], i.e., replacement of the guanidine $-NHC{=}NH(NH_2)$ with an urea $-NHC{=}O(NH_2)$, leads to a significant decrease in potency. Replacement of the ω' imino function in Arg with the carbonyl group in Cit results in a system with similar H bonding ability, but, unlike the Arg guanidine, the Cit urea is not charged under physiological conditions and therefore does not participate in ion pair interactions. Analysis of the peptide 5 complex crystal structure shows that the distance between Cit[1] NH and the Glu[220] side chain carbonyl O is 5.1 Å, whereas the corresponding distance in the peptide 4 structure is 4.5 Å. This difference effectively results in loss of the contacts between Glu[220] and the Cit-containing peptide. A similar picture emerges from comparison of the average cyclin A Glu[220] side chain atom B factors in both the peptide 5 and peptide 2 complex structures. In the latter structure, this factor lies only 20.5% above the average for all main chain atoms, whereas, in the unliganded and peptide 5-liganded complexes, the value rises to 45% and 67%, respectively. This is a clear indication of large displacement of Glu[220] side chain atoms when peptide 5 binds in the CBG.

Another factor contributing to the decrease in activity is the loss of intramolecular contacts with Leu[3]. The peptide 5 $2F_o - 1F_c$ map shows an absence of density for the Leu[3] side chain beyond the Cβ atom, indicating free rotation about the Cα-Cβ bond. By contrast, all atoms of the Leu[3] side chain are clearly visible in the electron density difference maps for the peptide 2 and peptide 4 structures (Figure 3). Apart from these differences at P^1 and P^3, the positions of the remaining atoms are similar, including the P^5 side chain conformation.

The effect of acetylation of the N-terminal nitrogen was also investigated. In the peptide 2 complex structure, the peptide amino terminus forms an H bond (3 Å) with the carbonyl of Ile[281] and a similar H bond is also observed in peptide 4 and peptide 3 structures. The weakening of this H bond (3.4 Å) upon acetylation of the peptide N terminus is consistent with the reduced biological activity of acetylated peptides (Table 2). An additional interesting observation relating to this involves the Arg[1] side chain, which cannot make the same contacts in the acetylated and nonacetylated peptides. In the acetylated peptide, a series of contacts are observed that are absent in peptides with free N termini and involve the acetyl O, a water molecule, the Glu[220] side chain, as well as the NH group of the Arg[1] side chain.

P^2 Site

Analysis of the peptide activity data for different amino acid residues in this position suggests that it is comparatively tolerant of modification. This finding is supported by the complex structures, which do not show any strong interactions between the P^2 side chain and the protein. In contrast to P^1, replacement of the charged side chain at P^2 has comparatively little effect on biological activity, as is apparent from the Arg[2]-Cit mutation. Inclusion of certain uncharged residues at P^2 is also tolerated to some extent, e.g., Gln (Table 2) or Ser (McInnes et al., 2003). The observed 3-fold reduction in potency, however, is consistent with the decrease in the Coulombic interaction energies calculated upon substitution of the Arg[2] with Asn.

P^3 Site

The necessity of a hydrophobic side chain at this position, as indicated by the activity data, is obvious from all structures reported here. The Leu[3] side chain participates in a network of van der Waals contacts with Gln[254], Trp[217], and Leu[214] of cyclin A, in addition to several intramolecular contacts with P^1 and P^5 (Figures 4B and 4C). Inspection of the complex structures and molecular modeling suggest that the Leu side chain is the optimum size for this position. Mutation of Ile is tolerated, but results in bad contacts and mutation to Ala leads to significant loss of potency. The Leu[3] side chain forms

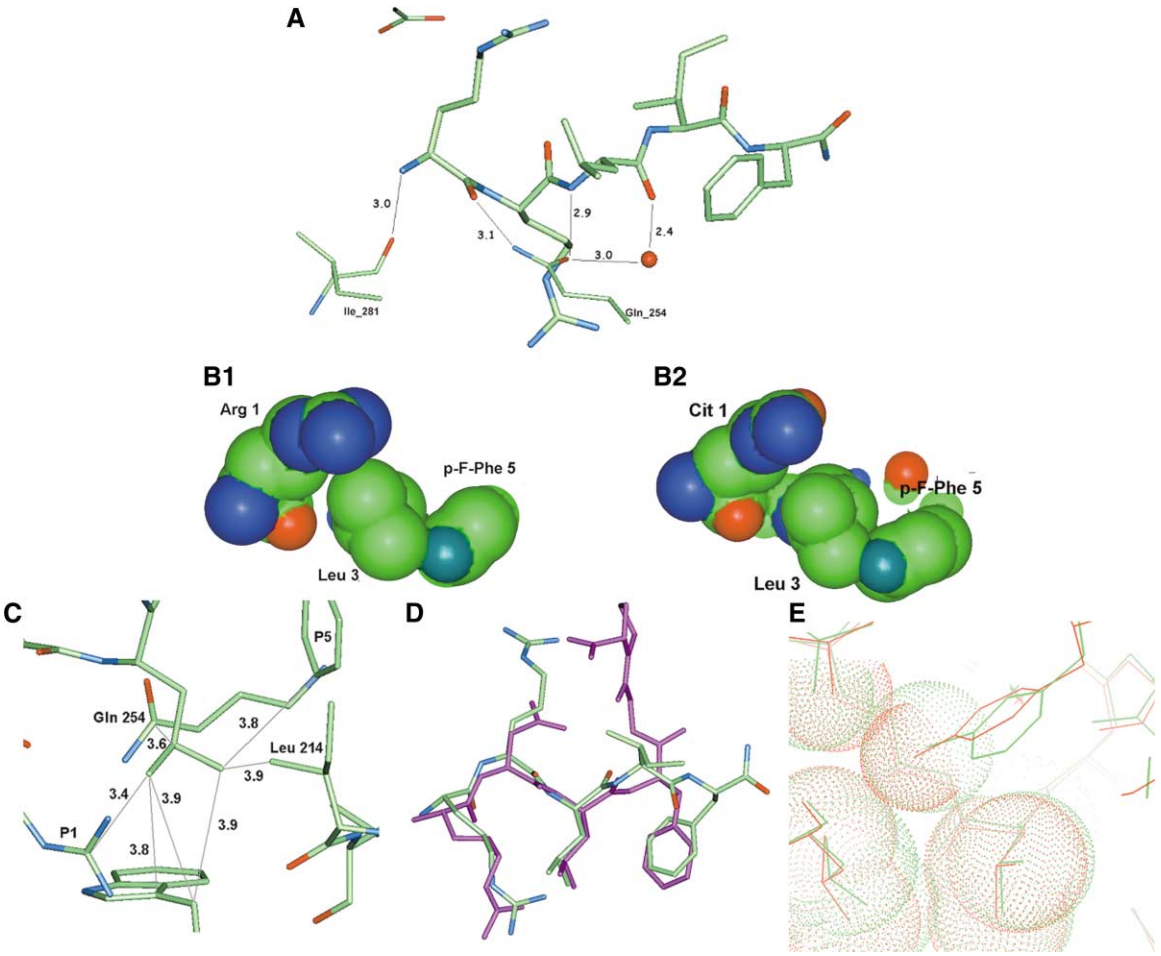

Figure 4. Inter and Intramolecular Interactions of Peptides 2, 3, 4, and 5

(A) H bonds involving the backbone of peptide 2.

(B) Effect of P^1 side chains: A charged P^1 side chain affects the position and flexibility of the Leu^3 side chain through van der Waal contacts, effectively locking the Leu^3 side chain between side chains P^1 and P^5. Mutation at P^1 from Arg (B1) to Cit (B2) results in a more flexible side chain at P^1, leading to a removal of the Leu^3 lock, whose side chain is now more flexible (refer Figure 3, electron density map 5).

(C) Contacts of the Leu^3 side chain in the peptide 2 structure.

(D) Superimposition of the cyclin A-bound H-Arg-Arg-Leu-Ile-Phe-NH_2 (CPK coloring) peptide and the corresponding $p27^{KIP1}$ peptide segment ^{30}Arg-Asn-Leu-Phe-Gly^{34} (magenta; PDB accession code 1JSU).

(E) Van der Waals surfaces of the Ac-Arg-Arg-Asn-(*m*-Cl-Phe)-NH_2 (green) and peptide 4 (red) complex structures surrounding the Phe^5 site. The fluorine and chlorine surfaces match exactly at the interface with the cyclin A surface.

the core of the binding surface for all of the peptides investigated and a residue with a side chain of lesser bulk in this position would allow the side chains at P^1 and P^5 to move freely. This in turn would result in disruption of the bound conformation, similar to the effect described above for P^1, but with a more profound result since now both neighboring side chains and their protein contacts would be affected.

P^4 Site

The major role of this residue (as encountered in the $p21^{WAF1}$ and p53 CBMs) is to act as a linker between the P^3 and P^5 hydrophobic groups. Incorporation of a linker is favorable for binding and in the peptides tested improves potency relative to the $p27^{KIP1}$ CBM, where the P^4 residue is absent (Leu^3-Phe^5-Gly^6). The extra three atoms of the Ile^4 residue in the backbone structure allow P^5 to adopt a more favorable position in the groove and make more complementary contacts with the hydrophobic pocket (Figure 4D). Also, as is discussed in the following section, the linker residue allows a more favorable intramolecular peptide conformation of the Leu^3 and Phe^5 residues. In addition, the Ile^4 spacing residue allows the P^3 carbonyl in peptide 2 to form a strong water-mediated H bond (2.4 Å) with the Gln^{254} side chain (Figure 4). In contrast, this carbonyl in the $p27^{KIP1}$ complex structure is rotated by almost 180° (Figure 4) and consequently this H bond is not present. These observations are backed up by the biochemical data since removal of Ile^3 results in 12-fold lower potency (Table 2). Furthermore, comparison of the structural data confirms that, due to the different conformations of the Phe^5 side chain, the *p*-F-Phe phenyl ring substitution is less effective in the context of the Leu-Phe-Gly sequence; the same modification of the aromatic side chain of Phe^5

Table 2. Peptide Structure-Activity Relationships Summary

Modifications at Position	Sequence	IC_{50} (μM) Competitive Cyclin A Binding	IC_{50} (μM) CDK2/Cyclin A Kinase Activity
1	**Ac**-Arg-Arg-Leu-Asn-(*p*-F-Phe)-NH_2	2.0	12
	H-Arg-Arg-Leu-Asn-(*p*-F-Phe)-NH_2	0.53	7.2
	H-**Arg**-Cit-Leu-Ile-(*p*-F-Phe)-NH_2	0.59	0.52
	H-**Cit**-Cit-Leu-Ile-(*p*-F-Phe)-NH_2*	21	37
2	H-Arg-**Arg**-Leu-Ala-(*p*-F-Phe)-NH_2	0.73	8.1
	H-Arg-**Cit**-Leu-Ala-(*p*-F-Phe)-NH_2	2.6	24
	H-Arg-**Gln**-Leu-Ile-(*p*-F-Phe)-NH_2	24	8.3
	H-Arg-**Cit**-Leu-Ile-(*p*-F-Phe)-NH_2	0.59	0.52
3	H-His-Ala-Lys-Arg-Arg-**Leu**-Ile-Phe-NH_2	0.05	0.14
	H-His-Ala-Lys-Arg-Arg-**Ala**-Ile-Phe-NH_2	1.5	>50
4	H-Cit-Cit-Leu-**Ile**-(*p*-F-Phe)-NH_2*	21	37
	H-Cit-Cit-Leu-**Ala**-(*p*-F-Phe)-NH_2	79	12
	H-Cit-Cit-Leu-**Asn**-(*p*-F-Phe)-NH_2	19	37
	H-Arg-Arg-Leu-**Ile**-Phe-NH_2*	0.68	7.7
	H-Arg-Arg-Leu- — -Phe-NH_2	8.1	>50
	H-Arg-Arg-Leu-**Asn**-(*p*-F-Phe)-NH_2	0.53	7.2
	H-Arg-Arg-Leu- — -(*p*-F-Phe)-NH_2	19	50
5	Ac-Arg-Arg-Leu-Asn-**Phe**-NH_2	12	>50
	Ac-Arg-Arg-Leu-Asn-(***p*-F-Phe**)-NH_2	2.0	12
	Ac-Arg-Arg-Leu-Asn-(***m*-Cl-Phe**)-NH_2*	5.6	31
	Ac-Arg-Arg-Leu-Asn-(***p*-Cl-Phe**)-NH_2	1.8	13

*Peptides with CDK2/CA complex structures.

results in considerable potency gains in the Leu-X-Phe motif (Table 2). In all of the structures reported here, the P^4 side chain does not make any contacts with cyclin A. Despite this observation, peptide potency does depend to some extent on the nature of P^4. A β-substituted side chain is preferred, presumably as it favorably reduces peptide flexibility in the unbound state.

P^5 Site

This site was probed with a variety of residues leading to the conclusion that certain aromatic side chains are optimal (McInnes et al., 2003). The most potent Phe derivatives were found to be *para* substituted (Table 2). The crystal structures of three peptides in which P^5 is *m*-Cl-Phe or *p*-F-Phe in complex with the cyclin A groove demonstrate that P^5 always occupies the same site (Figure 4E). The P^5 side chain in peptide 3 adopts a different conformation to that in the other structures (Figure 4B). Here the *meta*-chloro group forces the Phe^5 ring into a different conformation. As a consequence, it forms bad contacts with Met^{210}; these are offset, however, by the more favorable interactions of the chloro group with the base of the lipophilic pocket. The observed contacts with this pocket are so specific that the chlorine and fluorine van der Waals surfaces coincide very closely in the two superimposed peptide structures, despite the differing positions of the aromatic rings (Figure 4E). This observation reinforces the optimal substitution position of the P^5 phenyl ring as being *para*, a result reflected by the peptide activity data (Table 2).

Computational Analysis

In an attempt to better understand the observed differences in affinity for $p21^{WAF1}$- versus $p27^{KIP1}$-derived CBM peptides, intermolecular nonbonded energetics were calculated using the X-ray complex structures of the peptide 2 ($p21^{WAF1}$) and H-Arg-Asn-Leu-Phe-Gly-OH 4 (p27KIP1; PDB, 1H27) peptide (Lowe et al., 2002) (Table 3). The results help to explain the individual contributions for the $p21^{WAF1}$ and $p27^{KIP1}$ CBM peptides in terms of binding energy and indicate that a major contribution to the observed difference in affinity is due to the presence of a second charged Arg at P^2 in $p21^{WAF1}$. Although this residue does not appear to make specific protein contacts, it does contribute significantly via Coulombic energy due to its proximity with Asp^{283}. In addition, there also appears to be considerable contribution to binding from the surrounding solvent-mediated H bonds. Whereas the $p27^{KIP1}$ peptide structure (Russo et al., 1996) contains a single water molecule interacting with the peptide, we refined our structures to include as many crystallographically defined water molecules as could be found, especially in the binding groove, for the purpose of using these in drug design. Specifically, the energetic analysis suggests that a water-mediated H bond from the Leu^3 carbonyl to the Gln^{254} side chain provides 14 kcal/mol to the binding energy of the $p21^{WAF1}$ sequence. We also carried out energy minimization calculations on the bound conformations for peptide 2 and the H-Arg-Arg-Leu-Phe-NH_2 peptide in isolation from cyclin A. The energy difference between the minimized peptide conformation and that observed when bound to the CBG is an indication of the energetic penalty a peptide has to pay during binding. Since peptide 2 has to form nonoptimal intramolecular contacts and torsion angles in order to form complementarity with the cyclin groove, there is an unfavorable enthalpic contribution to the overall free energy. This was shown from the observation that the energy difference between the bound and minimized bound peptides was much greater for the $p27^{KIP1}$ (54 kcal/mol) versus the $p21^{WAF1}$ sequence (17 kcal/mol). As the binding energetics are comparable for peptide 2 and H-Arg-Arg Leu-Phe-NH_2, this factor most likely explains

Table 3. Comparison of Binding Energies and Torsion Angles of $p21^{WAF1}$- and $p27^{KIP1}$-Derived CBM Peptides

Interaction Energy (kcal/mol)				Torsion Angle (°)					
Peptide	1	2	3	Angle	Ideal Values	$p21^{WAF1}Ile^4$	$p21^{WAF1}Phe^5$	$p27^{KIP1}Leu^3$	$p27^{KIP1}Phe^4$
Coulombic	−323	−122	−286	φ	65.3		52		86
Van der Waals	−59	−59	−59	χ_1	64.1		72		38
Total (cyclin A − peptide)	−383	−181	−345	χ_2	177		134		81
Total (solvated cyclin A − peptide)	−410	−194	−356	ω	180	178	—	171	—
H_2O-bridged H bond*	−14								
Individual residues									
P^1	−107	−104	−104						
P^2	−66	−5.5	−50						
P^3	−7.4	−4.3	−4.7						
P^4	0.40	−12	−12						
P^5	−11	−1.1	−1.5						
P^6 (Pro)		−36							

Peptides: (1) H-Arg-Arg-Leu-Ile-Phe-NH_2; (2) H-Arg-Asn-Leu-Phe-Gly-OH; (3) H-Arg-Arg-Leu-Phe-NH_2.
*Water-bridged H bond between the peptide Leu^3 (CO) and Gln^{254} side chain (Fig. 4a) present only in $p21^{WAF1}$ motif.

the more than 10-fold potency decrease for the latter peptide. Those two peptides adopt a very similar conformation for the first three residues up to Leu^3 (Figure 4D). The main differences between the bound conformations are observed after Leu^3. These differences are the result of nonideal values for the intramolecular contacts in the $p27^{KIP1}$ versus the $p21^{WAF1}$ bound peptides, which also reflects the less favorable φ, χ_1, χ_2, and ω torsion angles of Leu^3 and Phe^4 for the $p27^{KIP1}$ peptide (Table 3). While these energetic calculations are obviously approximate, they nonetheless provide insight into the potency differences between cyclin groove inhibitor peptides.

Conclusion

The technique of ligand exchange was shown here to be an effective way of obtaining crystallographic information on series of compounds without having to depend on successful cocrystallization. As has been highlighted, many proteins do not yield crystals in the absence of suitable ligands. In the case studied, the use of a suitable starting ligand allowed the formation of crystals, which were subsequently employed to provide structural information for numerous ligands. The results reported here suggest that the ligand exchange approach may be of general use in different protein systems where native protein crystals are not readily obtainable, for example when contacts of surface-bound ligands with neighboring molecules are required for crystallization.

The peptides contain residues that are not directly involved in binding but act as spacers and help to orient those groups involved in groove recognition. The charged amino terminus and side chain functions at P^1 (Arg) are of prime importance for potency in the context of pentapeptide inhibitors. Replacement of the charged guanidine function with the uncharged isosteric urea group (Cit) and acetylation of the N terminus lead to ~36-fold and 3.8-fold potency reductions, respectively. The importance of the P^1-charged side chain is less pronounced in the octapeptide inhibitor series (McInnes et al., 2003), where the loss of the charge-charge interaction is partially offset by other favorable interactions not available in the pentapeptides. A second charged residue present at P^2 in CBMs can be eliminated more readily, due to the lesser contribution to binding. Although the side chain of Arg^2 does not form direct contacts with the cyclin groove, it clearly participates in long-range electrostatic interactions. Arg at P^2 can be effectively replaced, e.g., with Cit or Gln, and with other residues capable of both donating and accepting H bonds. The Leu residue at P^3 is invariant in all known CBMs and our results confirm that the Leu side chain optimally occupies the hydrophobic pocket at that site. The P^4 residue serves predominantly as a linker and a steric constraint. As it does not form any direct interactions with the protein, it is a potential candidate for modifications designed to improve the physicochemical characteristics of future inhibitors. Finally, P^5 is preferably an aromatic residue with a halogen-substituted phenyl group. The crystal structures and potency data indicate that occupying the volume filled by the halogen atoms makes important contributions to binding and hence should be accounted for in ligand design. Molecular modeling shows that there is sufficient space around this ring in the hydrophobic groove pocket to accommodate additional substituents, which could further increase the buried surface and hence the potency.

Overall, we have shown that peptide potency can be regained after truncation of the $p21^{WAF1}$ octapeptide and that a molecule with a lower net charge can be obtained through incorporation of unnatural amino acids. The structural basis for these improvements was rationalized and suggests that the development of small molecule inhibitors of the CDK2/CA via the substrate binding site is feasible. The important features of both the binding site and bound peptides incorporating nonnatural residues found during our work should facilitate the design of more potent and less peptidic inhibitors.

Experimental Procedures

Expression and Purification of CDK2, Cyclin A, and CDK2/CA Complex

Human recombinant CDK2 was expressed and purified as described (Wu et al., 2003). Human recombinant cyclin A2 (fragment encom-

passing residues 173–432) was expressed in *Escherichia coli* BL21 (DE3) using PET expression vectors. BL21 (DE3) was grown at 37°C with shaking (200 rpm) to mid-log phase ($A_{600nm} \approx 0.6$). Expression was induced by the addition of IPTG at a final concentration of 1 mM and the culture was incubated for a further 3 hr. Bacteria were harvested by centrifugation, and the cell pellet was resuspended in buffer A (25 mM Tris [pH 8.0], 5 mM DTT, 1 mM PMSF, 1 mM EDTA, 1 mM benzamidine, and protease inhibitor cocktail). After sonication the lysate was clarified by centrifugation for 30 min at 15,000 × g and 4°C. The supernatant was passed through a DEAE-Sepharose column (preequilibrated with buffer B: 25 mM Tris [pH 8.0], 2 mM DTT, 1 mM PMSF, 1 mM EDTA, 1 mM benzamidine, and 10 mM NaCl). After washing, bound protein was eluted with an ascending concentration gradient of NaCl in buffer B. The fractions containing cyclin A (typically eluted at 300–400 mM NaCl) were pooled, diluted (5 times in buffer A without protease inhibitor cocktail), and loaded on to a preequilibrated (with buffer B) SP-Sepharose column. After washing, bound protein was eluted with a NaCl gradient in buffer B. The fractions containing cyclin A (typically eluted at 300–400 mM NaCl) were pooled, diluted (5 times in buffer A without protease inhibitor cocktail), and loaded on to a preequilibrated (with buffer B) High-Trap Q column. After washing, bound protein was eluted with a NaCl gradient in buffer B. Pooled fractions containing pure cyclin A were mixed in a 1:1 molar ratio with CDK2 and were concentrated before loading on to a preequilibrated (with 50 mM Tris [pH 8.2], 100 mM NaCl, 1 mM EDTA, 1 mM DTT) Superdex 75 SE column. Eluted fractions containing stoichiometric mixtures of CDK2 and cyclin A were used for crystallization after concentration by ultrafiltration (Amicon concentration unit).

Crystallization and Structure Determination

The CDK2/CA/peptide crystals were grown by vapor diffusion using the hanging drop method. The peptides H-Arg-Arg-Leu-Ile-Phe-NH_2 and H-Arg-Arg-Leu-Ile-(*p*-F-Phe)-NH_2 were cocrystallized with CDK2/CA. Typically, a 2 μl solution of CDK2/cyclin A (7–8 mg/mL in 40 mM HEPES [pH 7.0], 200 mM NaCl, 5 mM DTT) and containing a 5-fold molar excess of peptide was mixed with 2 μl of well solution. The precipitant solution contained 18% PEG-3350 and 100 mM trisodium citrate. Crystals were obtained after 1–2 weeks at 17°C. CDK2/CA complexes with Ac-Arg-Arg-Leu-Asn-(*m*-Cl-Phe)-NH_2, H-Cit-Cit-Leu-Ile-(*p*-F-Phe)-NH_2, and H-Ala-Ala-Abu-Arg-Ser-Leu-Ile-(*p*-F-Phe)-NH_2 were prepared by a ligand exchange technique using CDK2/CA/H-Arg-Arg-Leu-Ile-Phe-NH_2 complex crystals. Initially, the exchange technique was carried out in two steps. First, H-Arg-Arg-Leu-Ile-Phe-NH_2 peptide was eluted from the crystal after soaking in a solution containing 18% PEG-3350 and 100 mM trisodium citrate. The unliganded crystal was then soaked in 18% PEG-3350, 100 mM trisodium citrate, and 1 mM of one of the above peptide. Later experiments showed that elution of H-Arg-Arg-Leu-Ile-Phe-NH_2 and soaking of a new peptide could be performed simultaneously. The final protocol consisted of soaking of CDK2/CA/peptide A crystals in mother liquor plus 1 mM peptide B for 3 days. The soaking solution (~10 μL) was replaced and the mixture stirred regularly during the soaking period. Under the experimental conditions used here, one crystal was soaked in a 10 μl drop of a 1 mM exchange peptide solution. This corresponds to less than 5 pmol of CDK2/CA mixed with 10 nmol of exchange peptide. Assuming a simple bimolecular equilibrium, the dissociation constant (K_c) between the ligand L and the protein P crystal is given by: $K_c = ([P_{unbound}][L_{unbound}])/[PL]$. This can be simply related to crystallographic (Wu et al., 2001) occupancy (Q) by $K_c = (1 - Q) \times [L_{free}]/Q$. Thus, for K_c values between 1 and 100 μM, and assuming unrestricted access to the cyclin ligand binding sites in the crystal, crystallographic occupancies would be expected to be greater than 90%.

Crystals of about 0.05 × 0.1 × 0.1 mm were mounted in 0.05–0.1 mm cryo-loops (Hampton Research). The crystals were immersed briefly in a cryoprotectant (28% PEG-3350 and 0.1 M trisodium citrate) and then flash-frozen in liquid nitrogen. Data were collected at the Daresbury (UK) and Grenoble (France) synchrotron facilities. Data processing was carried out using the program DENZO and SCALEPACK (Otwinowski and Minor, 1997), or MOSFLM (Leslie, 1992) and SCALA (Evans, 1993) from the CCP4 program suite (CCP, 1994). Data often showed signs of crystal radiation damage. The structures were solved by molecular replacement using MOLREP (Vagin and Teplyakov, 1997) and PDB entries 1HCL or 1CKP as the search model. ARP/wARP (Lamzin and Wilson, 1997) was used for initial density interpretation and the addition of water molecules. REFMAC (Murshudov et al., 1997) was used for structural refinement. A number of rounds of refinement and model building with the program Quanta (Accelrys, San Diego, USA) were carried out.

Computational Chemistry

Calculation of protein ligand interaction energies for the cyclin A inhibitors was performed using the program CDISCOVER after addition of hydrogens and steepest-descent minimization, using the modeling package InsightII (Accelrys, San Diego, USA).

Peptide Synthesis

Peptides were prepared, purified, and characterized using procedures as previously described (Zheleva et al., 2002).

Biochemical Assays

These were carried out as previously described (Atkinson et al., 2002; McInnes et al., 2003; Zheleva et al., 2002).

Acknowledgments

We would like to thank the staff of beamlines ID 14.1 and 14.2 at ESRF, as well as the staff of beamlines 14-1 and 14-2 at SRF Daresbury, for their assistance.

Received: July 10, 2003
Revised: August 22, 2003
Accepted: September 3, 2003
Published: December 2, 2003

References

Atkinson, G.E., Cowan, A., McInnes, C., Zheleva, D.I., Fischer, P.M., and Chan, W.C. (2002). Peptide inhibitors of CDK2-cyclin A that target the cyclin recruitment-site: structural variants of the C-terminal Phe. Bioorg. Med. Chem. Lett. *12*, 2501–2505.

Ball, K.L., Lain, S., Fåhraeus, R., Smythe, C., and Lane, D.P. (1996). Cell-cycle arrest and inhibition of Cdk4 activity by small peptides based on the carboxy-terminal domain of p21WAF1. Curr. Biol. *7*, 71–80.

Bonfanti, M., Taverna, S., Salmona, M., D'Incalci, M., and Broggini, M. (1997). p21WAF1-derived peptides linked to an internalization peptide inhibit human cancer cell growth. Cancer Res. *57*, 1442–1446.

Brown, N.R., Noble, M.E., Endicott, J.A., Garman, E.F., Wakatsuki, S., Mitchell, E., Rasmussen, B., Hunt, T., and Johnson, L.N. (1995). The crystal structure of cyclin A. Structure *3*, 1235–1247.

Brown, N.R., Noble, M.E., Endicott, J.A., and Johnson, L.N. (1999). The structural basis for specificity of substrate and recruitment peptides for cyclin-dependent kinases. Nat. Cell Biol. *1*, 438–443.

Chen, J., Saha, P., Kornbluth, S., Dynlacht, B.D., and Dutta, A. (1996). Cyclin binding motifs are essential for the function of p21CIP1. Mol. Cell. Biol. *16*, 4673–4682.

Chen, Y.-N.P., Sharma, S.K., Ramsey, T.M., Jiang, L., Martin, M.S., Baker, K., Adams, P.D., Bair, K.W., and Kaelin, W.G. (1999). Selective killing of transformed cells by cyclin/cyclin-dependent kinase 2 antagonists. Proc. Natl. Acad. Sci. USA *96*, 4325–4329.

Collaborative Computional Project (1994). The CCP4 suite: programs for protein crystallography. Acta Crystallogr. *D50*, 760–763.

Evans, R.R. (1993). Data reduction. In Proceedings of CCP4 Study Weekend on Data Collection and Processing, L. Sawyer, N. Isaacs, and S. Bailey, eds. (Science and Engineering Research Council UK: Daresbury Laboratory, Warrington), pp. 114–122.

Fischer, P.M. (2001). Recent advances and new directions in the discovery and development of cyclin-dependent kinase inhibitors. Curr. Opin. Drug Disc. Dev. *4*, 623–634.

Fischer, P.M., and Lane, D.P. (2000). Inhibitors of cyclin-dependent kinases as anti-cancer therapeutics. Curr. Med. Chem. *7*, 1213–1245.

Fischer, P.M., Krausz, E., and Lane, D.P. (2001). Cellular delivery

of impermeable effector molecules in the form of conjugates with peptides capable of mediating membrane translocation. Bioconjugate Chem. *12*, 825–841.

Fischer, P.M., Endicott, J., and Meijer, L. (2003). Cyclin-dependent kinase inhibitors. In Progress in Cell Cycle Research, L. Meijer, A. Jézéquel, and M. Roberge, eds. (Roscoff, France: Editions de la Station Biologique de Roscoff), pp. 235–248.

Jeffrey, P.D., Russo, A.A., Polyak, K., Gibbs, E., Hurwitz, J., Massague, J., and Pavletich, N.P. (1995). Mechanism of CDK activation revealed by the structure of a cyclinA-CDK2 complex. Nature *376*, 313–320.

Lamzin, V.S., and Wilson, K.S. (1997). Automated refinement for protein crystallography. Methods Enzymol. *277*, 269–305.

Lees, J.A., and Weinberg, R.A. (1999). Tossing monkey wrenches into the clock: new ways of treating cancer. Proc. Natl. Acad. Sci. USA *96*, 4421–4423.

Leslie, A.G.W. (1992). Recent changes to the MOSFLM package for processing film and image plate data. Joint CCP4 + ESF-EAMCB Newsletter on Protein Crystallography *26*.

Lowe, E.D., Tews, I., Cheng, K.Y., Brown, N.R., Gul, S., Noble, M.E.M., Gamblin, S.J., and Johnson, L.N. (2002). Specificity determinants of recruitment peptides bound to phospho-CDK2/cyclin A. Biochemistry *41*, 15625–15634.

McInnes, C., Andrews, M.J.I., Zheleva, D.I., Lane, D.P., and Fischer, P.M. (2003). Peptidomimetic design of CDK inhibitors targeting the recruitment site of the cyclin subunit. Curr. Med. Chem. Anti-Cancer Agents *3*, 57–69.

Mendoza, N., Fong, S., Marsters, J., Koeppen, H., Schwall, R., and Wickramasinghe, D. (2003). Selective cyclin-dependent kinase 2/cyclin A antagonists that differ from ATP site inhibitors block tumor growth. Cancer Res. *63*, 1020–1024.

Munshi, S., Chen, Z., Li, Y., Olsen, D.B., Fraley, M.E., Hungate, R.W., and Kuo, L.C. (1998). Rapid X-ray diffraction analysis of HIV-1 protease-inhibitor complexes: inhibitor exchange in single crystals of the bound enzyme. Acta Crystallogr. *D54*, 1053–1060.

Murshudov, G.N., Vagin, A.A., and Dodson, E.J. (1997). Refinement of macromolecular structures by the maximum-likelihood method. Acta Crystallogr. *D53*, 240–255.

Ortega, S., Malumbres, M., and Barbacid, M. (2002). Cell cycle and cancer: the G1 restriction point and the G1/S transition. Curr. Genomics *3*, 245–263.

Otwinowski, Z., and Minor, W. (1997). Processing of x-ray diffraction data collected in oscillation mode. Methods Enzymol. *276*, 307–326.

Russo, A.A., Jeffrey, P.D., Patten, A.K., Massague, J., and Pavletich, N.P. (1996). Crystal structure of the p27Kip1 cyclin-dependent-kinase inhibitor bound to the cyclin A-Cdk2 complex. Nature *382*, 325–331.

Schulman, B.A., Lindstrom, D.L., and Harlow, E. (1998). Substrate recruitment to cyclin-dependent kinase 2 by a multipurpose docking site on cyclin A. Proc. Natl. Acad. Sci. USA *95*, 10453–10458.

Vagin, A., and Teplyakov, A. (1997). MOLREP: an automated program for molecular replacement. J. Appl. Crystallogr. *30*, 1022–1025.

Wohlschlegel, J.A., Dwyer, B.T., Takeda, D.Y., Dutta, A. (2001). Mutational analysis of the Cy motif from p21 reveals sequence degeneracy and specificity for different cyclin-dependent kinases. Mol Cell Biol. *21*, 4868–4874.

Wu, S.-Y., Dornan, J., Kontopidis, G., Taylor, P., and Walkinshaw, M.D. (2001). The first direct determination of a ligand binding constant in protein crystals. Angew. Chem. Int. Ed. *40*, 582–586.

Wu, S.Y., McNae, I., Kontopidis, G., McClue, S.J., McInnes, C., Stewart, K.J., Wang, S., Zheleva, D.I., Marriage, H., Lane, D.P., et al. (2003). Discovery of a novel family of CDK inhibitors with the program LIDAEUS: structural basis for ligand-induced disordering of the activation loop. Structure *11*, 399–410.

Zheleva, D.I., McInnes, C., Gavine, A.-L., Zhelev, N.Z., Fischer, P.M., and Lane, D.P. (2002). Highly potent $p21^{WAF1}$ derived peptide inhibitors of CDK-mediated pRb phosphorylation: delineation and structural insight into their interactions with cyclin A. J. Pept. Res. *60*, 257–270.

Accession Numbers

Structures have been deposited in the Protein Data Bank under ID codes 1OKU, 1OKV, 1OKW, 1OL2, and 1OL1 for the CDK2/CA complexes with peptides 1–5.